Fundamental Photoelectrocatalytic and Electrophoretic Mobility Studies of TIO_2 and V-Doped TIO_2 Thin-Film Electrode Materials

Jeosadaque J. Sene,† Walter A. Zeltner, and Marc A. Anderson*

Environmental Chemistry and Technology Program, University of Wisconsin-Madison, 660 North Park Street, Madison, Wisconsin 53706

Received: June 17, 2002

Titanium dioxide and vanadium-doped titanium dioxide prepared by the sol−gel method showed a quantum-size effect in the form of a 0.19 eV blue shift in the band gap energy compared to bulk TiO_2. The presence of vanadium as a dopant did not affect the band gap energy of TiO_2. However, concentrations of this dopant up to 1% atom ratio increased the pH of the isoelectric point (IEP) above the value of 5.8 found for pure TiO_2. When the vanadium concentration surpassed 1%, the IEP began to decrease, dropping below the IEP of pure TiO_2 at dopant concentrations greater than ca. 2%. Thin-film electrodes fabricated from TiO_2 and V-doped TiO_2 coated on titanium foil showed different performances in degrading formic acid and oxalic acid depending on the V content in the catalyst. Using the 5% V-doped TiO_2 electrode, 82% of TOC was removed from an aqueous solution containing oxalic acid (25 mg L^{-1} in C) against 74% removed by the pure TiO_2 thin-film electrode in 1 h. In degrading formic acid, 79% of TOC was removed using the 1% V-doped photoelectrode against 77% removed using the plain TiO_2 in 1 h. Additionally, the influence of the bias potential on photoelectrocatalytic oxidation using these thin-film electrodes is discussed as well as the effect of metal doping on the flat band potential of the electrodes.

Introduction

Titanium dioxide has been one of the most widely employed photocatalytic semiconducting materials since the early seventies when Fujishima and Honda[1] demonstrated the feasibility of splitting water by using a simple photoelectrochemical cell. This experiment employed a single-crystal TiO_2 electrode as a photoanode that was illuminated with light of wavelength less than 350 nm. Since then, titanium dioxide has been found to have appropriate physical and chemical properties for research applications not only in water splitting[2] but also in solar energy conversion,[3−5] energy storage,[6−7] fuel cells,[8−9] and environmental decontamination.[10−13] Despite the many advantages of TiO_2, numerous studies have been conducted to overcome the striking disadvantage of its high band gap energy (3.2 eV) that prohibits this semiconductor from absorbing a large part of the solar energy spectrum reaching the earth.[14−19]

The sol−gel process of molecular doping has proven to be effective in preparing new TiO_2-based catalysts that either absorb visible light or have better conducting characteristics under band gap irradiation. Doping introduces minute amounts of a foreign element (usually less than 5% atom ratio) to the bulk TiO_2 in the expectation that some atoms of the foreign element will substitute for some titanium atoms in the lattice of the oxide. Other methods for doping[20,21] have been reported but have the disadvantage of using complicated and high cost techniques. Unlike these techniques, sol−gel doping[22,23] is a simple, inexpensive method that can produce a highly homogeneous distribution of almost any transition or nontransition element into TiO_2. These new metal-doped catalysts can easily be supported on many types of substrates to yield highly porous ceramic materials having several applications.[11−13]

In this paper, we present the results of doping TiO_2 with vanadium at several atom ratios using the sol−gel method. Physical properties were investigated by electrophoretic mobility, XRD analysis, and UV−visible spectroscopy. Photoelectrochemical parameters such as band gap energy and flat band potential were investigated by electrochemical techniques such as linear sweep voltammetry (LSV) and controlled potential electrolysis (CPE). We also report the results of photoelectrocatalytic degradation of organic molecules in an aqueous medium over thin-film electrodes fabricated from these new catalysts. These results will indicate if V-doped TiO_2 prepared by a sol−gel process will display a lower band gap energy than pure TiO_2 and if V-doped TiO_2 will provide larger photocurrents as well as better performance as a photoelectrocatalyst than TiO_2.

Experimental Section

Preparation of Catalysts and Photoelectrodes. Titanium (IV) ethoxide (Gelest) and vanadium (V) triisopropoxide oxide (Alfa Aesar) were used as precursors for preparing undoped- and V-doped TiO_2 colloidal suspensions. Typically, the required volume of the doping reagent (enough for 0.5%, 1.0%, 2.5%, and 5.0% atom ratios) was added under argon to 10 mL of titanium ethoxide, which was diluted with 10 mL of anhydrous ethanol. The mixture was stirred for 48 h and then hydrolyzed in enough 0.15 mol L^{-1} HNO_3 aqueous solution to keep the ratio of $H_2O/Ti/H^+$ at 200/1/0.5. Immediately after adding the alkoxide mixture to the nitric acid solution, the alcohol was boiled off at 80 °C, and the sol was stirred until a stable colloidal suspension was obtained, which typically required about 2 days.

* To whom correspondence should be addressed. Phone: (608) 262 2674. Fax (608) 262 0454. E-mail: nanopor@facstaff.wisc.edu.

† Present address: Fundação Educacional de Barretos, Av. Prof. Roberto Frade Monte, 389, CEP 14783-226, Barretos-SP, Brazil. E-mail: jeosa@si.feb.br.

10.1021/jp026317y CCC: $25.00
Published on Web 01/22/2003

This suspension was then dialyzed against ultrapure water to pH $\approx$ 3.5 by using a Spectra/Por 3 regenerated cellulose membrane (Spectrum Medical Industries, Inc.) with a molecular weight cutoff of 3500 daltons.[23] These processing steps remove most of the organics from the suspension. Pure TiO_2 suspensions were prepared following the same methods in order to compare these materials to the V-doped catalysts. Thin-film photoelectrodes were dip-coated onto a titanium foil back contact (0.05 or 0.5 mm thick, Goodfellow Cambridge Ltd), after heating the Ti foils at 350 °C, according to a procedure described earlier.[11] The photoelectrodes were heated again at 350 °C after each coating.

Test Cells. Photocurrent measurements and flat band potential determinations were carried out using a 30-mL single-compartment Teflon cell having a circular quartz window of 50-mm diameter. A circular opening in the cell opposite the quartz window allowed exposure of 4.5 cm^2 of the working electrode (TiO_2 or V-doped TiO_2) to UV illumination. The platinum foil counter electrode (9.0 cm^2), having a circular opening of the same size as the light pathway, was placed just in front of the working electrode, 1 cm away. A saturated calomel electrode (SCE), used as a reference, was placed close to the working electrode through a bridge tube with a Vycor frit tip.

The photoelectrocatalytic degradation experiments were performed in a two-compartment reactor. A Nafion 117 membrane was used to separate both compartments while allowing electrolyte contact. The photoactive area of the anode (TiO_2 or V-doped TiO_2) was 10 cm^2 that was illuminated by a 450 W Xe−Hg arc lamp (Oriel, model 6262) UV light source through a quartz circular window mounted in one side of the cell. The compartment containing the platinum counter electrode of approximately the same area was not directly exposed to the UV illumination. The reference electrode was the same SCE mentioned above. A Princeton Applied Research (PAR) potentiostat model 6310 was used to bias the photoanode in the photoelectrocatalytic experiments and also to record the LSV plots for measuring photocurrents. All LSV measurements employed a voltage sweep of 10 mV/s.

All experiments employed the same UV light source. The irradiance at the working electrode surface was 50 mW cm^{-2}, as measured with an International Light Inc. model IL 1400A photometer.

X-ray Diffraction. A Scintag Padv diffractometer using Cu $K\alpha_1$ and Cu $K\alpha_2$ was used to record X-ray patterns from powder samples fired at 350 °C.

Electrophoresis Measurements. Electrophoretic mobility of pure TiO_2 and V-doped TiO_2 nanoparticles were measured with a Malvern Instruments Zetasizer, model 3000HS, from suspensions 2.5×10^{-3} mol L^{-1} in TiO_2. Hydrogels were formed from the suspensions by allowing the solvent to evaporate, after which the hydrogels were heated at 350 °C. The resulting solids were then finely ground and suspended in 0.01 mol L^{-1} KNO_3 as an inert electrolyte. The pH was adjusted under N_2 atmosphere with aqueous solutions of HNO_3 or KOH. Suspensions were kept standing overnight, and the pH was rechecked prior to each measurement. The equipment was standardized before use with a latex particle suspension with a known zeta potential of 50 $\pm$ 5 mV.

UV−Visible Spectroscopy. Absorption spectra in the ultraviolet and visible range were recorded with a Hewlett-Packard model HP 8452A spectrophotometer. Quartz slides were dip-coated with the suspensions of the catalysts and fired at 350 °C for 3 h before measurement.

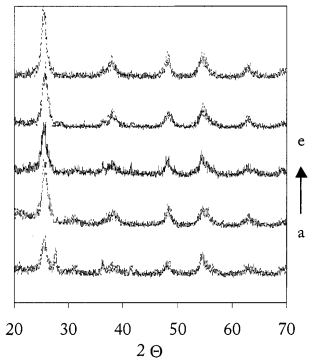

Figure 1. X-ray diffraction patterns of the photocatalyst materials fired at 350 °C for 3 h: (a) TiO_2; (b) 0.5%V−TiO_2; (c) 1.0%V−TiO_2; (d) 2.5%V−TiO_2; (e) 5.0%V−TiO_2.

Results and Discussion

Crystal Structure Patterns. Transition metal ions incorporated as dopants into other compounds may distort the crystal lattice of the doped material. To evaluate the changes that vanadium might cause to the crystal structure of TiO_2, we recorded X-ray diffraction patterns (Figure 1) for the V-doped and undoped TiO_2 powders fired at 350 °C for 3 h. Except for some peaks attributable to the rutile phase in the undoped TiO_2, all other reflections are attributable to anatase. It has been observed in previous work[15,24] that niobium and vanadium stabilize the anatase crystalline form of TiO_2 (i.e., the temperature for the anatase to rutile phase transition increases in the doped materials). As can be seen in Figure 1, this observation held for these photocatalytic materials, because the rutile phase is not detected even in samples with vanadium content as low as 0.5% atom ratio. No diffraction peaks originating from V_2O_5 crystallites were detected. Based on data presented in Rodella et al.,[25] we believe that all vanadium is dispersed throughout TiO_2 as vanadyl groups (V^{4+}) and/or polymeric vanadates (V^{5+}) rather than crystalline V_2O_5. (These authors identified at least three families of V^{4+} ions in their study.) They also observed a strong influence of the firing temperature on the form of vanadium in V-doped titania samples prepared by the sol−gel method. Only vanadyl groups and polymeric vanadates were detected in samples that were fired up to 500 °C. When the doped samples were fired above 600 °C, the vanadyl groups tended to polymerize and form crystalline V_2O_5. This effect is probably related to the decrease in surface area associated with the anatase to rutile phase transition that also occurred at these high firing temperatures. Because our samples were fired at 350 °C, it is reasonable to assume that the vanadium is dispersed homogeneously in the TiO_2 film either as V^{4+} or polymeric V^{5+}.

Electrophoresis Measurements. Electrophoretic mobility of TiO_2 and the V-doped TiO_2 nanoparticles dispersed in a 0.01 mol L^{-1} KNO_3 aqueous solution was measured as a function of pH. Figure 2 shows these results, including the mobility of a sample of pure V_2O_5 also prepared by the sol−gel method. The isoelectric point (IEP) was found to be at pH 5.8 for pure TiO_2 and increased with the amount of vanadium doping up to a 1% atom ratio. For those samples containing more than 1% vanadium, the IEP started to decrease, eventually dropping below 5.8 at a doping level of about 2%. These changes in IEP as a function of the vanadium concentration are shown in the inset of Figure 2. (Note that a measurement has been included for a sample of material that contains 1.4% V.) As discussed in the previous section, vanadyl groups (V^{4+}) and polymeric V^{5+} vanadate are likely prevalent in V-doped TiO_2 samples fired at

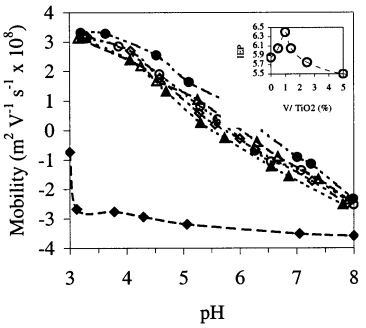

Figure 2. Electrophoretic mobility curves for nanocrystalline particles of TiO_2 and V-doped TiO_2 dispersed in 0.01 mol L^{-1} KNO_3: (○) TiO_2; (△) 0.5%V−TiO_2; (●) 1.0%V−TiO_2; (◇) 2.5%V−TiO_2; (▲) 5.0%V−TiO_2; (◆) V_2O_5.

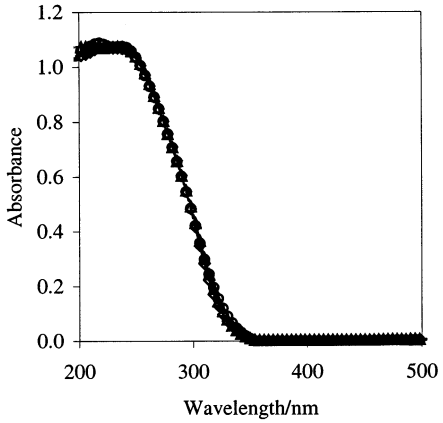

Figure 3. UV-visible spectra of TiO_2 and V-doped TiO_2 films coated on quartz substrates. Film thickness ≈ 100 nm. (○) TiO_2; (◆) 1.0%V−TiO_2; (◇) 5.0%V−TiO_2.

temperatures lower than 500 °C.[25] These results show that, at concentrations of vanadium up to 1%, the polymeric V^{5+} vanadate with its extra positive charge increases the positive charge of the surface of the doped material, thereby increasing the IEP above that of pure TiO_2. As the concentration of vanadium increases above 1%, the surface starts to lose positive charge, and the IEP shifts toward that of pure V_2O_5, which was determined to be pH 2.0. We speculate that, at higher doping concentrations of vanadium, some polymeric vanadate (V^{5+}) converts to crystalline V_2O_5.

UV−Visible Spectra and Band Gap Energy. To estimate the band gap energy of the pure TiO_2 and the V-doped samples, thin films were prepared by dip-coating square pieces of quartz slides (2 × 2 cm) with the sols. One layer of the nanocrystalline semiconducting material was estimated to be 100 nm thick in previous work.[12] The slides were then fired at 350 °C for 3 h in order to be compared with the actual thin-film electrodes used in the photoelectrocatalytic experiments. The UV−vis spectra were recorded using a blank slide as a reference and are presented in Figure 3. Independently of the content of vanadium doping, no shift is observed in the profile of the absorption spectra. All samples show an onset of absorption at 360 nm.

The band gap energy was determined from the absorption coefficient (α) calculated by eq 1, using the measured values of absorbance (A) at each wavelength of interest and a film thickness (d) of 100 nm:[26]

$$\alpha = 2.303\frac{1}{d}A \qquad (1)$$

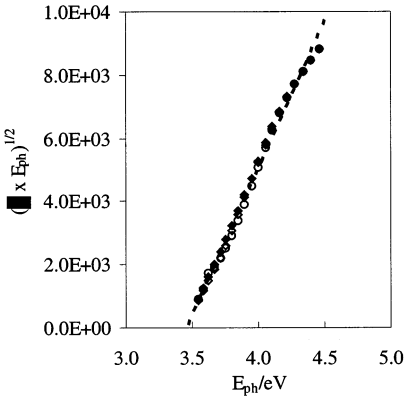

Figure 4. Band gap determination of TiO_2 and V-doped TiO_2 films coated on quartz substrates. Film thickness ≈ 100 nm. (○) TiO_2; (◆) 1.0%V−TiO_2; (◇) 5.0%V−TiO_2.

For a semiconductor in which the band energy has a parabolic structure, eq 2 relates the absorption coefficient and the photon energy (E_{ph}):[27]

$$\alpha = B(E_{ph} - E_{bg})^n/E_{ph} \qquad (2)$$

In eq 2, B is a constant with a value between 10^4 and 10^6, n is either 0.5 for a direct band-band transition or 2 for an indirect transition, and E_{bg} is the band gap energy. Accordingly, for a direct transition of titanium dioxide, a plot of $(\alpha E_{ph})^{1/2}$ vs E_{ph} should yield a straight line and the band gap energy can be determined from the intercept. Figure 4 shows this determination for TiO_2, 1%V−TiO_2, and 5%V−TiO_2. A straight line was obtained for all semiconductors with a constant $B = 10^4$ determined from the slope, in good agreement with other reported values.[26] E_{bg} for all samples was found to be 3.44 eV, that is, a blue shift of 0.19 eV from the bulk-phase band gap for anatase (3.25 eV).[28]

Kormann et al.[29] employed a quantum mechanical approach based on a theoretical prediction of Brus[30] to estimate a blue shift (ΔE_{bg}) of 0.15 eV for TiO_2 nanoparticles with a characteristic dimension of 1.2 nm. Choi et al.[31] found a blue shift of 0.17 eV for their 2.2 nm colloidal TiO_2 using the same quantum mechanical treatment. Separately,[32] they determined that suspensions of quantum-sized TiO_2 particles with dimensions of 2−4 nm showed an equivalent band-gap transition at 360 nm, which corresponds to 3.44 eV, the same value we report. Therefore, regardless of their vanadium content, all samples prepared by the sol−gel method displayed quantum-size effects. According to elementary quantum mechanics, when the size of the semiconductor particles is comparable to or smaller than the de Broglie wavelength, the density of electronic states decreases, causing the allowed energy states to become discrete rather than continuous.[26] Size measurements carried out by using photon correlation spectroscopy revealed that the particle size of our suspended TiO_2 nanoparticles lies in the domain of 5−10 nm. This observation suggests that these suspended particles are aggregates of primary particles with characteristic dimensions of ca. 2 nm.

Photocurrent Measurements. Photocurrents associated with these photoelectrodes as a function of applied potential were investigated in aqueous solutions of 0.5 mol L^{-1} NaCl by recording LSV curves. A profile of such curves is shown in Figure 5 for the pure TiO_2 thin-film electrode at pH 3 and 11, as well as the dark current in the background electrolyte. Typically, under UV illumination, an n-type semiconductor electrode such as TiO_2 produces a high anodic current at

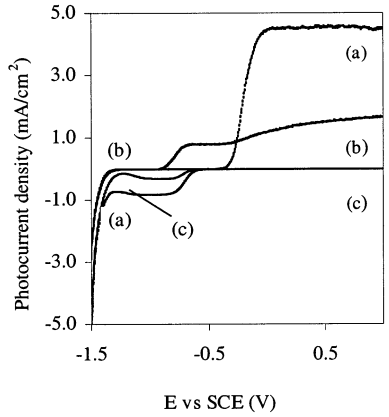

Figure 5. Photocurrent−potential curves for pure TiO_2 thin-film electrodes in 0.5 mol L^{-1} NaCl at (a) pH 3.0, (b) pH 11.0, and (c) dark current in the background electrolyte.

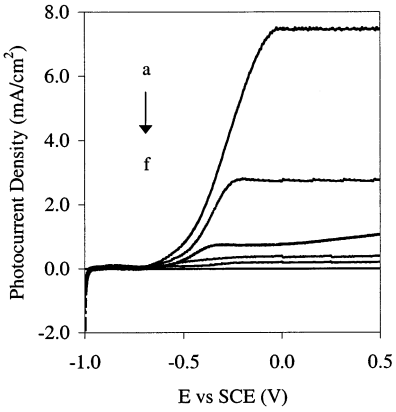

Figure 6. Photocurrent−potential curves for TiO_2 and V-doped TiO_2 photoelectrodes in aqueous solution containing 0.1 mol L^{-1} formic acid in 0.5 mol L^{-1} Na_2SO_4: (a) TiO_2; (b) 1%V−TiO_2; (c) 0.5%V−TiO_2; (d) 2.5%V−TiO_2; (e) 5%V−TiO_2; (f) dark current in the background electrolyte.

potentials positive to the flat band potential. Increasing the pH causes the flat band potential to shift to more negative values. Although the flat band potential is independent of the electrolyte, the intensity of the photocurrent is influenced by the efficiency of the species acting as a hole scavenger. At pH 3.0, the main species acting as a hole scavenger is the Cl^- anion because the electrode surface is positively charged in the absence of an applied potential. As a result, HOCl is produced, as postulated recently.[33] However, at pH 11 the electrode surface is negative when there is no applied potential. Therefore, the adsorption of Cl^- on this surface is unfavorable. In this case, the concentration of OH^- is sufficiently high for this species to act as a hole scavenger with the resulting formation of $OH^\bullet$ radicals. When compared to HOCl production, the formation of $OH^\bullet$ radicals leads to a smaller photocurrent density.

To further investigate the effect of the electrolyte on photocurrent, we recorded voltammograms for all of the photoelectrodes in an aqueous solution containing 0.1 mol L^{-1} formic acid in 0.5 mol L^{-1} Na_2SO_4 (initial pH $\approx$ 3.7). Formic acid can be easily oxidized on TiO_2 photoelectrodes,[11,12] and sodium sulfate does not produce as high a background photocurrent as sodium chloride.[33] The results of these measurements are shown in Figure 6. An even higher photocurrent is observed for the TiO_2 photoelectrode in this system than in 0.5 mol L^{-1} NaCl at pH 3.0 because of the oxidation of formic acid. However, the photocurrent for all of the V-doped TiO_2 photoelectrodes is smaller than that observed for pure TiO_2. Except for the 1%V−TiO_2, the photocurrents for the other V-doped catalysts are quite small, probably because of charge recombination caused by the introduction of surface states between the valence and conduction bands.

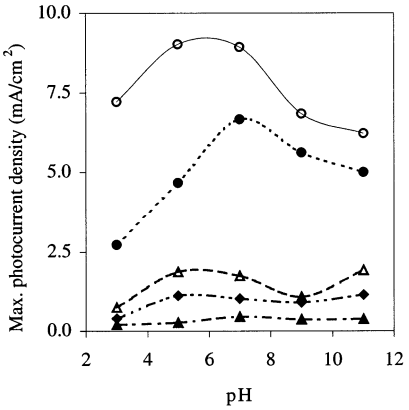

Figure 7. Maximum photocurrent density as a function of pH for TiO_2 and V-doped TiO_2 photoelectrodes measured in 0.5 mol L^{-1} NaCl: ○) TiO_2; (△) 0.5%V−TiO_2; (●) 1.0%V−TiO_2; (◆) 2.5%V−TiO_2; (▲) 5.0%V−TiO_2.

The influence of pH on the maximum photocurrent generated by all of the photoelectrodes in 0.5 mol L^{-1} NaCl is presented in Figure 7. Although the performance of the 1%V−TiO_2 photoelectrode is also influenced by the aforementioned surface states, its higher photocurrents as compared to the other doped photoelectrodes are striking. It may be that the higher pH of its isoelectric point compensates for the loss in the photocurrent due to charge recombination.

Flat Band Potential and Band Edge Positions. Differently from the photocatalytic approach, charge carriers (electrons and holes) in a photoelectrocatalytic cell are split off, with electrons being driven to the cathode through the external conductor and holes being consumed by the hole-scavenger species present in the electrolyte. Accordingly, both half-cell reactions occur separately from one another rather than at the same site, as is characteristic of most photocatalytic experiments. Our photoelectrochemical system consisted of a semiconductor electrode (plain TiO_2 or V-doped TiO_2 layered onto titanium foil), an electrolyte containing the electroactive species, the inert counter electrode (platinum), and a reference electrode (SCE).[34] By simultaneously biasing the photoanode and exciting the semiconductor with light of wavelength lower than the band gap (<360 nm), the photogenerated charge carriers are kept apart as long as an effective hole scavenger in the anode half-cell compartment can prevent charge recombination. In this case, the electrons flow from the conduction band through the back metal contact and are driven off to the cathode.[34] Then, for the half-reaction occurring on the photoanode, the following equation can be written:

$$TiO_2(s) + H_2O + h^+ \xrightarrow{h\nu} TiO_2 - OH^\bullet(s) + H^+(aq) \quad (3)$$

The minority charge carriers photogenerated upon illumination can oxidize the water producing $OH^\bullet$ radicals that adsorb on the photoelectrode surface with the release of H^+ ions to the solution. Thus, the reaction depends on the pH of the solution according to the following Nernst equation:

$$E_{fb} = E^\circ_{fb} + \frac{RT}{nF}\log\frac{1}{[H^+]} \quad (4)$$

where E°_{fb} is the flat band potential at pH 0. Because one

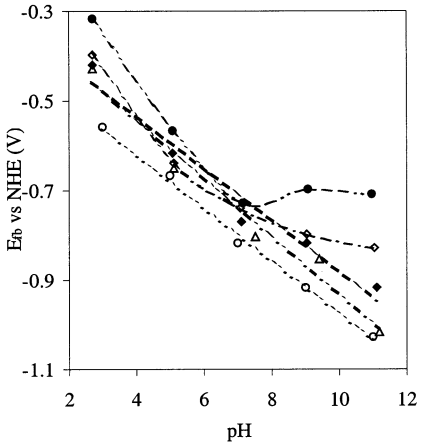

Figure 8. Flat band potential as a function of pH for TiO_2 and V-doped TiO_2 photoelectrodes in 0.5 mol L^{-1} NaCl: (○) TiO_2; (◆) 0.5%V−TiO_2; (△) 1.0%V−TiO_2; (◇) 2.5%V−TiO_2; (●) 5.0%V−TiO_2.

electron per photon is produced during excitation of the semiconductor, one obtains for a Nernstian process occurring at 25 °C:

$$E_{fb} = E^{\circ}_{fb} + 0.06\ \mathrm{pH} \qquad (5)$$

We used the method of the onset of the photocurrent[28] to measure the flat band potential for the photoelectrodes fabricated from TiO_2 and V-doped TiO_2. Figure 8 shows the plots for the flat band (E_{fb}) potential as a function of the pH of the solution. Although the E_{fb} values were measured against the SCE as a reference, we have converted them to be referenced to the normal hydrogen electrode (NHE). As can be seen in Figure 8, the flat band potential of TiO_2 follows a Nernstian behavior with a slope of −59 mV and an intercept for pH 0 equal to −0.38 V (corresponding to E_{fb} at pH 0 of −0.62 V vs SCE). This value does not agree well with reported values of about −0.2 V (vs SCE) for E_{fb} as extrapolated to pH 0,[36] measured using the method employed for this paper, or −0.4 V (vs SCE) at pH 0, measured using a UV−visible spectroscopic technique.[37] The V-doped photoelectrodes display similar Nernstian profiles at dopant levels up to 1% vanadium. When the concentration of vanadium surpasses 1%, the curves deviate from the Nernst equation, and the flat band potential becomes reasonably constant beyond the IEP of the semiconductor.

The intercepts of the curves in Figure 8 at pH 0 were used to estimate the position of the lower edge of the conduction band (CB) for each photoelectrode.[38] The position of the upper edge of the valence band (VB) was calculated by subtracting the value of the band gap energy (3.44 eV) from the value of the conduction band edge. Figure 9 shows a diagram with the energy correlations at the semiconductor−solution interface relative to the pure TiO_2 and the V-doped TiO_2 photocatalysts. The standard redox potentials for hydrogen and possible organic target species at pH 0 are also shown. Figure 9 reveals that the upper level of the valence band, which represents the oxidizing power of holes generated upon illumination, increases (i.e., becomes stronger) as the content of vanadium increases from pure TiO_2 to more doped photocatalysts. Then, in theory, it should be easier to oxidize reduced species whose standard potentials lie within the band gap, using a more heavily V-doped catalyst than pure TiO_2. However, other factors such as adsorption and charge recombination will also play an important role in the effectiveness of the final process.

Photoelectrocatalytic Degradation of Organic Pollutants. To test this hypothesis, thin-film electrodes fabricated from the

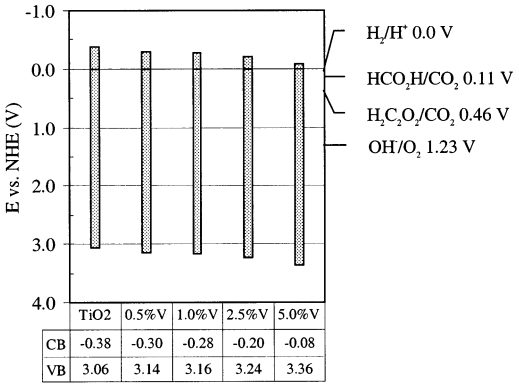

	TiO2	0.5%V	1.0%V	2.5%V	5.0%V
CB	-0.38	-0.30	-0.28	-0.20	-0.08
VB	3.06	3.14	3.16	3.24	3.36

Figure 9. Band edge positions for TiO_2 and V-doped TiO_2 and the standard redox potential for some species in water at pH 0. CB and VB stand for conduction band and valence band, respectively.

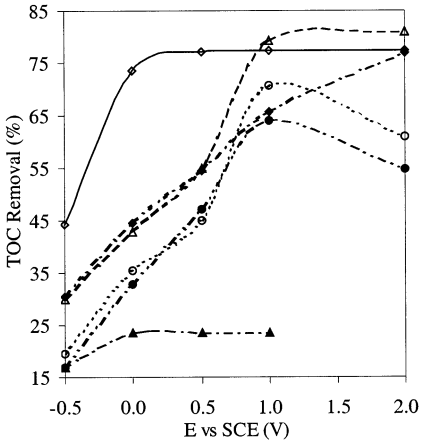

Figure 10. Photoelectrocatalytic degradation of 2.1×10^{-3} mol L^{-1} aqueous formic acid in 0.5 mol L^{-1} NaCl using TiO_2 and V-doped TiO_2 thin-film electrodes as a function of the bias potential during 1-h experiments: (◇) TiO_2; (◆) 0.5%V−TiO_2; (△) 1.0%V−TiO_2; (○) 2.5%V−TiO_2; (●) 5.0%V−TiO_2; (▲) V_2O_5.

TiO_2 and V-doped TiO_2 were tested for their ability to degrade two organic surrogate contaminants, i.e., formic acid and oxalic acid. We chose formic acid because of prior experience in the photoelectrocatalytic degradation of this species in our laboratory.[11,12] Oxalic acid was chosen because its standard potential is more positive than that of formic acid and lies deeper within the band gap of TiO_2. Figure 10 shows the results of the photoelectrocatalytic degradation of an aqueous solution of 2.1×10^{-3} mol L^{-1} formic acid in a 1-h period using the TiO_2 and V-doped TiO_2 thin-film electrodes as a function of the bias potential.

The undoped TiO_2 catalyst provides its best performance over a range of applied potentials from as low as 0.25 V (vs SCE) up to 2.0 V. Because the applied potential acts by minimizing recombination of the photogenerated charges, no improvement in the formic acid oxidation is observed by increasing the bias potential beyond +0.25 V. The 1%V−TiO_2 photoelectrode exhibits the best performance among the V-doped TiO_2 photocatalysts. Because the flat band potential of the V-doped TiO_2 materials is more positive than that of the pure TiO_2, the maximum formic acid degradation occurs only after higher applied potentials for all the doped photoelectrodes (typically +1 V or higher). However, for the 1%V−TiO_2 photoelectrode, the amount of formic acid degraded in 1 h is even higher than that obtained with pure TiO_2. We believe this observation indicates the influence of doping on the surface charge of the photocatalyst, as shown by the changes in IEP on doping (see

TABLE 1: Photoelectrocatalytic Degradation of Organic Surrogates (25 mg L^{-1} in C) over TiO_2 and V-doped TiO_2 Thin-Film Photoelectrodes in Triplicate 1-h Experiments at an Applied Potential of +1.0 V vs SCE[a]

catalyst	formic acid degradation (% of TOC removal)	oxalic acid degradation (% of TOC removal)
TiO_2	77.3 ± 0.6	74.4 ± 0.8
1%V−TiO_2	79.2 ± 0.6	75.9 ± 0.6
5%V−TiO_2	64.1 ± 0.8	81.6 ± 0.5

[a] The electrolyte was 0.5 mol L^{-1} NaCl.

Figure 2). Because adding up to 1% atom ratio vanadium to TiO_2 increases the IEP of the doped catalysts (i.e., makes their surfaces more positive), adsorption of negatively charged formate anions on these surfaces may be favored. The better performance of the 1%V-doped TiO_2 photoelectrode can then be explained by the synergistic effect of the shift in IEP and the maximum efficiency of the bias potential in minimizing charge recombination at applied potentials above +1 V (vs SCE). Such effects are not observed for the other V-doped photocatalysts, and the degradation is even poorer when using an electrode coated with only V_2O_5 (IEP at pH 2.0).

Table 1 shows the results of the degradation of formic acid ($E° = 0.11$ V) and oxalic acid ($E° = 0.46$ V) as the percentage of TOC removal in 1 h for triplicate measurements. Pure TiO_2 removed 3% more TOC from an aqueous solution of formic acid than from an aqueous solution of oxalic acid. The same result was found for the 1%V−TiO_2 photoelectrode, except that the latter performed slightly better than pure TiO_2. (In separate experiments not reported in Table 1, this trend was also observed for biasing potentials greater than 1.0 V.) Although the 5%V−TiO_2 photoelectrode degrades less formic acid than the others, it degrades more oxalic acid. We believe that this result can be explained by the shift in the flat band potential (therein in the position of the edge of the valence band), which results in a stronger oxidizing power of the photogenerated holes. Again, the synergistic effect of adsorption and the position of the flat band potential play a key role in the process. In this case, because a considerable number of oxalate ions bear a double negative charge, they probably adsorb better than the single negative formate anions. (The initial pH of the oxalic acid solution is 3.75 and the pK_2 value for oxalic acid is 4.19.)

Conclusions

Vanadium-doped titanium dioxide synthesized by the sol−gel method can be coated on titanium foil to fabricate thin-film electrodes with improved performance toward the photoelectrocatalytic oxidation of organic contaminants. Concentrations of vanadium up to 1% atom ratio shift the isoelectric point to higher pH values compared to pure TiO_2. When the vanadium concentration exceeds 1%, the IEP begins to decrease, shifting toward that of V_2O_5, which was determined to be at pH 2.0. These changes in the surface charge make each of the photocatalysts unique from the standpoint of the adsorption of organic species that can undergo photoelectrocatalytic oxidation.

The flat band potential is also affected by the presence of the doping metal. As a result, the position of the edge of the valence band is shifted to more positive potentials as the content of vanadium increases from pure TiO_2 to 5%V−TiO_2 (atom ratio), which increases the oxidizing power of the photogenerated holes. On the basis of these findings, we believe that the entire oxidative process on the electrode surface is determined by the vanadium content (which influences the adsorption and the position of the valence band), the bias potential on the electrode, and the standard potential of the species being reduced. In this sense, oxalate ($E° = 0.46$ V) is degraded more extensively with a heavily V-doped TiO_2 photoelectrode than with a pure TiO_2 photoelectrode.

In addition, the presence of vanadium does not influence the band gap energy of TiO_2. However, as the sol−gel method produces highly dispersed nanocrystalline particles, the band gap energy is larger than that of bulk TiO_2 as a result of quantum effects. This is in fact advantageous because holes with stronger oxidizing power are photogenerated at the surface. Additionally, these thin-film electrodes present high surface-to-mass ratios because of their nanoporous characteristics, which make them suitable for application in large-scale systems.

Acknowledgment. J. J. Sene thanks the financial support from Fapesp-Brazil. The authors wish to express their gratitude to Dr. M. I. Tejedor-Tejedor for her helpful discussions and suggestions on the UV-visible section.

References and Notes

(1) Fujishima, A.; Honda, K. *Nature* **1972**, *238*, 37.
(2) Fujihara, K.; Ohno, T.; Matsumura, M. *J. Chem. Soc., Faraday Trans.* **1998**, *94*, 3705.
(3) Arango, A. C.; Johnson, L. R.; Bliznyuk, V. N.; Schlesinger, Z.; Carter, S. A.; Horhold, H. H. *Adv. Mater.* **2000**, *12*, 1689.
(4) Hara, K.; Sayama, K.; Ohga, Y.; Shinpo, A.; Suga, S.; Arakawa, H. *Chem. Commun.* **2001**, *6*, 569.
(5) Suleymanov, A. S. *Int. J. Hydrogen Energ.* **1991**, *16*, 741.
(6) Peng, Z. Y.; Shi, Z.; Liu, M. L. *Chem. Commun.* **2000**, *21*, 2125.
(7) Xing, X. K.; Shi, M. L.; Yang, Q. H.; Wu, H. Q. *Acta Chim. Sinica.* **1982**, *40*, 201.
(8) Vichi, F. M.; Tejedor-Tejedor, M. I.; Anderson, M. A. *Chem. Mater.* **2000**, *12*, 1762.
(9) Hamnett, A.; Stevens, P. S.; Wingate, R. D. *J. Appl. Electrochem.* **1991**, *21*, 982.
(10) Hoffmann, M. R.; Martin, S. T.; Choi, W.; Bahnemann, D. W. *Chem. Rev.* **1995**, *95*, 69.
(11) Candal, R. J.; Zeltner, W. A.; Anderson, M. A. *J. Adv. Oxid. Technol.* **1998**, *3*, 270.
(12) Kim, D. H.; Anderson, M. A. *Environ. Sci. Technol.* **1994**, *28*, 479.
(13) Sun, C. C.; Chou, T. C. *Ind. Eng. Chem. Res.* **1998**, *37*, 4207.
(14) Iwasaki, M.; Hara, M.; Kawada, H.; Tada, H.; Ito, S. *J. Coll. Int. Sci.* **2000**, *224*, 202.
(15) Kikkawa, H.; O'Regan, B.; Anderson, M. A. *J. Electroanal. Chem.* **1991**, *309*, 91.
(16) Shiyanovskaya, I.; Hepel, M. *J. Electrochem. Soc.* **1999**, *146*, 243.
(17) Wilke, K.; Breuer, H. D. *J. Photochem. Photobiol. A: Chem.* **1999**, *121*, 49.
(18) Zang, L.; Lange, C.; Abraham, I.; Storck, S.; Maier, W. F.; Kisch, H. *J. Phys. Chem. B* **1998**, *102*, 10765.
(19) Tacconi, N. R.; Wenren, H.; Rajeshwar, K. *J. Electrochem. Soc.* **1997**, *144*, 3159.
(20) Daniele, S.; Bragato, C.; Battiston, G. A.; Gerbasi, R. *Electrochim. Acta* **2001**, *46*, 2961.
(21) Anpo, M.; Yamashita, H.; Ichihashi, Y. *Optronics* **1997**, *186*, 161.
(22) Anderson, M. A.; Gieselman, M. J. *J. Membr. Sci.* **1988**, *39*, 243.
(23) Xu, Q.; Anderson, M. A. *J. Mater. Res.* **1991**, *6*, 1073.
(24) Bischoff, B. L. *Thermal Stabilization of Anatase (TiO_2) Membranes*, Ph.D. Thesis, University of Wisconsin-Madison, Madison, WI, 1992.
(25) Rodella, C. B.; Nascente, P. A. P.; Franco, R. W. A.; Magon, C. J.; Mastelaro, V. R.; Florentino, A. O. *Phys. Stat. Sol. (A)* **2001**, *187*, 161.
(26) Memming, R. *Semicondutor Electrochemistry*; Wiley-VCH: Weinheim, Germany, 2001; Chapter 1.
(27) Pankove, J. I. *Optical Processes in Semiconductors*; Dover: New York, 1971; Chapter 3.
(28) Finklea, H. O. *Semiconductor electrodes*; Elsevier: New York, 1988; Chapter 2.
(29) Kormann, C.; Bahnemann, D. W.; Hoffmann, M. R. *J. Phys. Chem.* **1988**, *92*, 5196.
(30) Brus, L. *J. Phys. Chem.* **1986**, *90*, 2555.

(31) Choi, W.; Termin, A.; Hoffmann, M. R. *J. Phys. Chem*. **1994**, *98*, 13669.

(32) Choi, W.; Termin, A.; Hoffmann, M. R. *Angew. Chem., Int. Ed. Engl*. **1994**, *33*, 1091.

(33) Zanoni, M. V. B.; Sene, J. J.; Anderson, M. A. *J. Photochem. Photobiol. A: Chem.* **2002** (submitted).

(34) Sawyer, D. T.; Sobkowiak, A.; Roberts, J. L., Jr. *Electrochemistry for Chemists*, 2nd ed.; John Wiley & Sons: New York, 1995; Chapter 1.

(35) Graetzel, M. *Heterogeneous Photochemical Electron Transfer*; CRC Press: Boca Raton, FL, 1988; Chapter 3.

(36) Nelson, B. P.; Candal, R. J.; Corn, R. M.; Anderson, M. A. *Langmuir* **2000**, *16*, 6094.

(37) Redmond, G.; Fitzmaurice, D. *J. Phys. Chem.* **1993**, *97*, 1426.

(38) Morrison, R. S. *Electrochemistry at Semiconductor and Oxidized Metal Electrodes*; Plenum Press: New York, 1980; Chapter 4.